Available online at www.sciencedirect.com
ScienceDirect
Journal of the European Ceramic Society 30 (2010) 657–668
www.elsevier.com/locate/jeurceramsoc

Effect of cation doping on lattice and grain boundary diffusion in superplastic yttria-stabilized tetragonal zirconia

Marek Boniecki [a,*], Yuriy Natanzon [b], Zbigniew Łodziana [c,b]

[a] *Institute of Electronic Materials Technology, 133 Wólczyńska Str., 01-919 Warsaw, Poland*
[b] *The Henryk Niewodniczański Institute of Nuclear Physics Polish Academy of Sciences, 152 Radzikowskiego Str., 31-242 Cracow, Poland*
[c] *Department of Enviroment, Energy and Mobility EPMA, 8600 Dübendorf, Switzerland*

Received 8 January 2009; received in revised form 25 August 2009; accepted 10 September 2009
Available online 8 October 2009

Abstract

Lattice diffusion coefficients D_l and grain boundary diffusion D_{gb} coefficients of hafnium were studied for 0.5 and 1 mol% cation-doped yttria-stabilized tetragonal zirconia at the temperature range from 1283 to 1510 °C. The diffusion profiles were determined by two experimental techniques: secondary ion mass spectroscopy and electron microprobe analysis. Additionally the first principle calculations of the electronic states of Zr^{4+}, dopant cations and O^{2-} anions and elastic properties in 3Y-TZP were performed. Superplastic strain rate versus stress and inverse temperature was also measured. For 1 mol% doped samples the significant increase of the grain boundary diffusion and superplastic strain rate was observed. Correlations between the calculated ionic net charges and D_{gb} indicate that enhancement of D_{gb} was caused by the reduction of ionic bonding strength between metal cation and oxygen anion in zirconia. The new constitutive equation for superplastic flow of yttria-stabilized tetragonal zirconia ceramics was obtained.

Keywords: Zirconia; Diffusion coefficient; Tracer; Superplasticity; Dopant

1. Introduction

Diffusion plays an essential role in such phenomena observed in ceramics at high temperatures as: deformations under the influence of stresses (creep and superplasticity) or electric conductivity[1] observed in ceramics at high temperature. Analysis of the results concerning superplasticity in oxide ceramics presented in literature[2–8] lead to the conclusion, that the correct insight into these phenomena requires independently measured values of diffusion coefficients. One can mention three types of diffusion in polycrystalline materials: lattice, grain boundary and surface diffusion. The first and the second type of diffusion are important in dense materials but the last one is crucial for materials with large porosity.[1]

One of the most interesting structural materials is 3 mol% yttria-stabilized tetragonal zirconia (ZrO_2) polycrystals (3Y-TZP). Simultaneously 3Y-TZP with submicrometer grain size exhibits superplastic deformation at temperatures above 1200 °C.[2–7] Superplasticity creates an opportunity of easy shaping and joining of ceramic elements. However, at present the effect of cavitation followed by cracking of the ceramics during superplastic deformation is a serious limitations for broad application of this phenomenon in the ceramic technology. During the last years several studies have been reported in order to improve the situation. For example, addition of some oxides (as Al_2O_3, SiO_2, GeO_2, TiO_2, MgO) to 3Y-TZP significantly enhances the superplastic flow in this material.[9,10] Superplastic flow in 3Y-TZP is attributed to the grain boundary sliding controlled by the grain boundary diffusion of Zr^{4+} ions.[5] The dopant cations added to 3Y-TZP, tend to segregate to the grain boundaries, thus they could affect grain boundary diffusion of Zr^{4+} and hence they could change the superplastic flow of the ceramics. The diffusion coefficients in tetragonal ZrO_2 for Zr^{4+} were measured by Sakka et al.[11] and Swaroop et al.[12] However the data reported in Ref. 11 concern the 14 mol% CeO_2 stabilized zirconia but in Ref. 12. only pure 3Y-TZP is considered. Kuwabara et al.[13] reported that addition of Ti and Ge ions leads to reduction

* Corresponding author.
E-mail addresses: Marek.Boniecki@itme.edu.pl, Marek-Boniecki@wp.pl (M. Boniecki).

0955-2219/$ – see front matter © 2009 Elsevier Ltd. All rights reserved.
doi:10.1016/j.jeurceramsoc.2009.09.009

of the ionic bond strength between cation and oxygen ions in 3Y-TZP. They have supposed that it causes the enhancement of cation diffusion and hence the increase of superplastic flow of 3Y-TZP.

In the present paper we report on:

1. Determination of the lattice and grain boundary diffusion coefficients for pure and cation-doped 3Y-TZP.
2. Finding the relationship of the ionic bonding strength between zirconium and oxygen ions with diffusion coefficients for various dopants.
3. The correlation between the grain boundary diffusion and superplastic strain rate for various dopants.

2. Experimental procedure

Two methods of diffusion coefficient measurements were used:

1. With aid of the secondary ion mass spectrometry (SIMS) using samples with thin layer of hafnia deposited on their surfaces (Hf was chosen as a tracer for Zr[12]).
2. With aid of the electron microprobe analyser (EMA) by scanning the cross-section of diffusion couple 3Y-TZP and ZrO_2 + 10 mol% HfO_2 (Zr–Hf interdiffusion[11]).

The 3Y-TZP and ZrO_2 + 10 mol% HfO_2 composite materials were prepared. The following powders were used:

1. 3 mol% yttria-stabilized tetragonal ZrO_2 from Zhongshun Sci. & Tech., China. Besides HfO_2 (1.9 wt%) other impurity content did not exceed 0.05 wt% ($SiO_2 < 0.005$, $Al_2O_3 < 0.02$, $Fe_2O_3 < 0.006$ and $TiO_2 < 0.002$ wt% according to the technology specifications enclosed by the producer), crystallite size was 20–30 nm.
2. HfO_2 from Alfa Aesar GMBH, Germany. It contained 98.5 wt% HfO_2 and about 1.5 wt% ZrO_2, crystallite size was 0.5 ± 0.3 μm.
3. Al_2O_3 (AKP-53 type) from Sumitomo, Japan, impurity content was about 130 ppm and crystallite size was about 0.32 μm.
4. $MgAl_2O_4$ (spinel S30CR type) from Baikalox, France, impurity content was about 45 ppm and crystallite size was about 0.2 μm.
5. SiO_2, MgO, GeO_2, TiO_2 supplied by various producers, of purity 99.999%.

The batches of samples with 0.5 and 1 mol% of oxides (Al_2O_3, SiO_2, MgO, $MgAl_2O_4$, GeO_2, TiO_2), pure 3Y-TZP and zirconia–hafnia composite (containing 10 mol% of HfO_2) with and without dopants (only 1 mol%) were made. In order to obtain the samples ZrO_2 powder was mixed with chosen oxide powders by ball-milling method for 24 h in water. Subsequently, the powders were dried and uniaxially pressed under pressure of 20 MPa and then isostatically pressed at 120 MPa. Plates obtained by this method were sintered at 1350 °C for 2 h in air at a heating and cooling rate of 2 K/min. The samples of dimensions of: 4 mm × 11 mm × 1.5 mm and of 4 mm × 4 mm × 2.5 mm for diffusion measurements (accordingly for SIMS and EMA) and 2.5 mm × 2.5 mm × 5 mm for compression tests for superplasticity measurements were cut from the sintered plates. The samples for the diffusion measurements were polished and some of them were thermally etched at 1300 °C for 1 h in vacuum. The electron scanning microscope micrographs of the etched samples were used for measurements of average grain size by Feret's diameter method. Results of grain size measurements are shown in Table 1.

Table 1
Grain size d in μm for 0.5 and 1 mol% doped oxide 3Y-TZP and 1 mol% doped ZrO_2–10 mol% HfO_2.

Dopant oxide	3Y-TZP		ZrO_2–10 mol% HfO_2
	0.5 mol%	1 mol%	1 mol%
–	0.30 ± 0.06	–	0.25 ± 0.04
Al_2O_3	0.19 ± 0.09	0.36 ± 0.09	0.28 ± 0.09
SiO_2	0.23 ± 0.05	0.27 ± 0.07	0.32 ± 0.07
MgO	0.18 ± 0.12	0.28 ± 0.06	0.31 ± 0.09
$MgAl_2O_4$	0.27 ± 0.13	0.32 ± 0.04	0.32 ± 0.11
GeO_2	0.15 ± 0.08	0.34 ± 0.05	0.33 ± 0.09
TiO_2	0.18 ± 0.09	0.34 ± 0.08	0.31 ± 0.11

(–): means the undoped sample. Densities of all 3Y-TZP samples were larger than 97% of theoretical density which equals 6.1 g/cm^3 and for ZrO_2–10 mol% HfO_2 samples were larger than 94% of theoretical density which equals 6.45 g/cm^3.

For SIMS investigation of diffusion coefficients the thin film tracer of HfO_2 was deposited by sputtering from Hf target in an Ar + 17 wt% O_2 atmosphere on the polished surface of the samples. The amorphous films with thickness of about 30 nm were obtained. Diffusion anneals were carried out in air at 1510–1283 °C for 1–24 h. A Cameca IMS 6f SIMS was used with Cs^+ as a primary ion beam. In order to reduce charging the samples were coated with a thin gold layer. The crater depth was measured by a profilometer in order to convert sputter time into depth. The analysis area of the craters (about 200 μm × 200 μm) was large compared to the grain size so the measured intensities were proportional to the mean concentration c of the tracer (Hf) monitored at a given depth.

For investigation of diffusion coefficients with aid of EMA the polished surfaces of a pair of 3Y-TZP and zirconia–hafnia (undoped and 1 mol% doped) samples were joined together at temperature 1350 °C under the pressure of 20 MPa for 15 min using an universal testing machine with a furnace. Diffusion anneals were carried out at 1510–1355 °C for 72–312 h in air. The concentration distributions of Zr and Hf were determined using EMA Cameca SX-100 by scanning the cross-section of the diffusion couple perpendicularly to the diffusion direction. A spatial resolution of the EMA equalled 1 μm. Grain size of some samples was measured after diffusion annealing.

The superplasticity tests were performed in compression geometry under constant load in air at 1280–1500 °C and in the stresses range of 20–50 MPa using Zwick 1446 universal testing machine. A decrease in stress with an increase in compressive deformation was recorded. The maximum strains on the specimens attained values about 0.8. Strain rate $d\varepsilon/dt$ versus stress σ was calculated from experimental data according to Ref. 14.

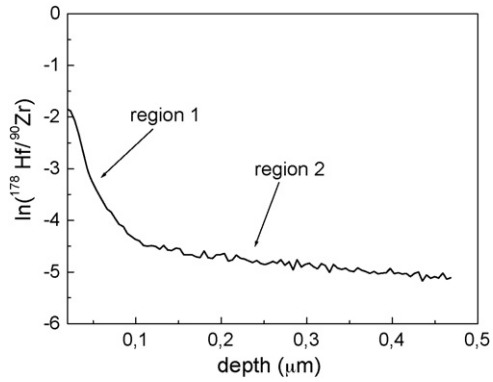

Fig. 1. The depth profile in terms of relative intensity of ^{178}Hf versus distance from the surface for undoped 3Y-TZP annealed at 1283 °C for 24 h.

3. Computational procedure

Calculations of electronic and elastic properties of doped 3Y-TZP were performed within density-functional theory (DFT)[15] implemented in SIESTA program.[16] We have used generalized-gradient approximation (GGA)[17] for exchange-correlation functional; the Plane-Wave cutoff of 476 eV (350 Ry) and the *k* point grid with a step of 0.03 Å.

The core electrons are described by effective norm-conserving potentials with Troullier and Martins parameterization.[18] In this work we have used GGA pseudopotentials in Perdew–Burke–Ernzerhof parameterization.[19] The valence configurations were $2s^2 2p^4$ for O, $3s^2 3p^2$ for Si, $4s^2 4p^2$ for Ge, $3s^2 3p^1$ for Al and $3s^2$ for Mg. In order to achieve better accuracy 4s and 4p core electrons of Zr/Y as well as 3s and 3p core electrons of Ti were treated as valence states and were not replaced by pseudopotentials. Thus the valence configurations were $4s^2 4p^6 5s^2 4d^2$ for Zr, $4s^2 4p^6 5s^2 4d^1$ for Y and $3s^2 3p^6 4s^2 3d^2$ for Ti. The supercell technique was used to various concentration of yttrium and other dopants as described in Ref. 20. The concentrations of Y and dopant oxides were the same depending on the size of the supercell (the smaller the cell the larger the concentration and vice versa). Such approach has limitations on the possible dopant concentrations as it can be changed only in defined finite steps. The Y/dopant concentrations were considered for of 2.8 mol% (for Al_2O_3 and MgO) because of the difficulty of introducing aliovalent dopant metal oxides into ZrO_2 and 6.7 mol% for the rest of dopants. The selected supercells contained accordingly 47 atoms for 6.7 mol% Y/dopant concentration and 107 atoms for 2.8 mol% Y/dopant. Elastic constants of pure and doped ZrO_2 were calculated by series of finite deformations of the supercells. More details interested reader can find in Refs. 20–22.

The net ionic charges were obtained by explicit integration of the ground state electron density around each atom over a sphere of selected radius.[23] The integration radius was 1.2 Å for Zr and O, 1.16 Å for Y, 1 Å for Ti, Ge, Si, Al and Mg. The choice of such radii was done in accordance to atoms electronegativities and the interatomic corresponding bond lengths.

4. Results

4.1. Diffusion coefficient measurements

An example of the data obtained from SIMS is presented in Fig. 1.

The lattice D_l and grain boundary D_{gb} diffusion coefficients were calculated respectively from regions 1 and 2 using Eqs. (1) and (2) from diffusion theory for instantaneous source boundary condition (thin layer of deposited tracer)[24,25]:

$$D_l = \left(-4t\frac{\partial \ln c}{\partial x^2}\right)^{-1} \quad (1)$$

where c means tracer concentration, t—annealing time, x—depth:

$$sD_{gb}\delta = 1.31\left(\frac{D_l}{t}\right)^{1/2}\left[-\frac{\partial \ln c}{\partial x^{6/5}}\right]^{-5/3} \quad (2)$$

where s—segregation factor (=1 for self-diffusion) and δ—the grain boundary width (=1 nm).

A plot of $\log(c)$ versus the square of the depth yields a straight line corresponding to region 1 as shown in Fig. 2a. The obtained slope was used to calculate D_l from Eq. (1). Similarly a plot of $\log(c)$ versus $x^{6/5}$ yields a straight line corresponding to region 2 (Fig. 2b) and hence the slope was used to calculate D_{gb} from Eq. (2). The procedure described above was carried out to evaluate the diffusion coefficients for other temperatures

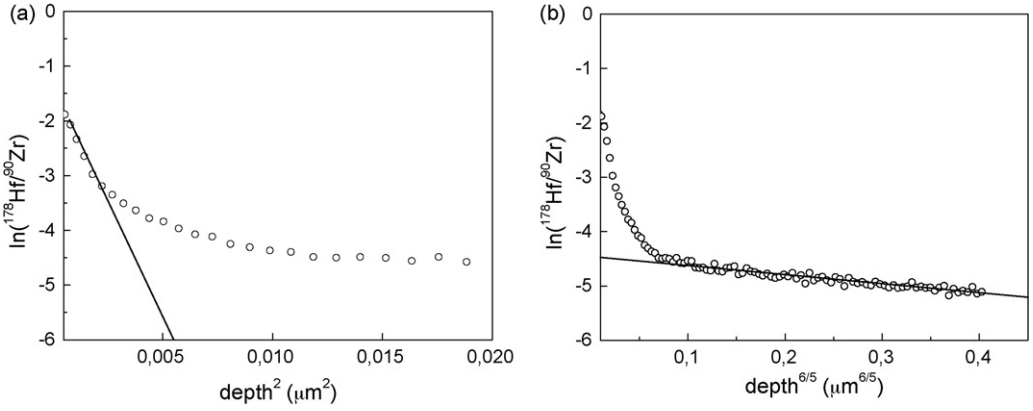

Fig. 2. Methods of lattice (a) and grain boundary diffusion coefficient (b) calculations for the example from Fig. 1.

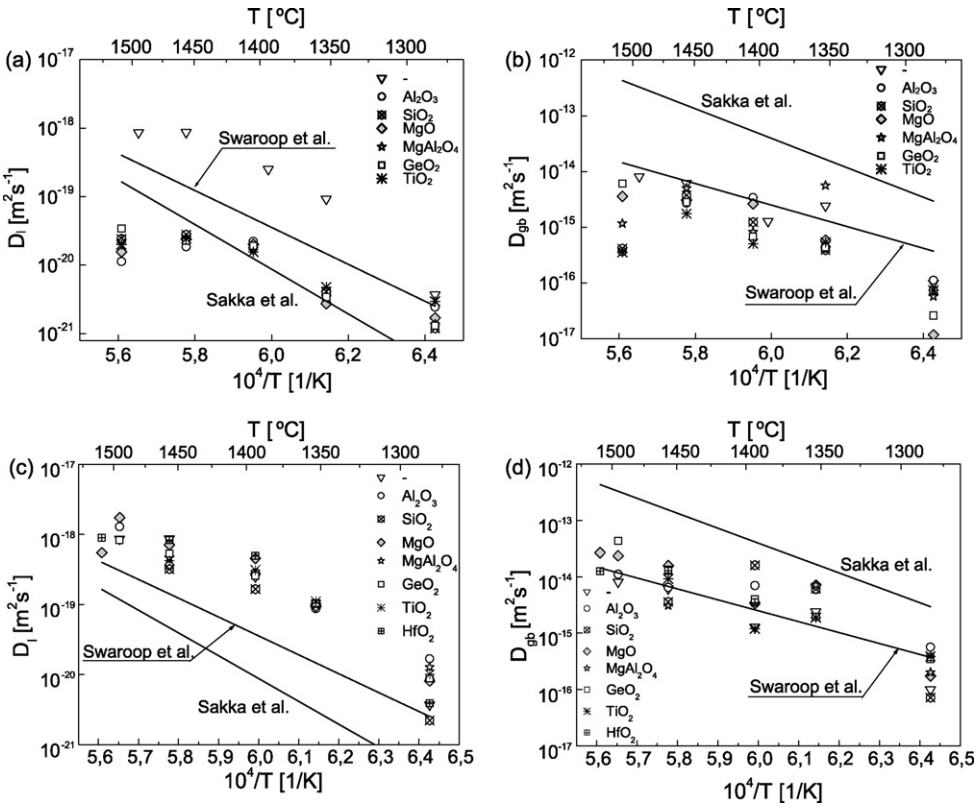

Fig. 3. Arrhenius plots of lattice D_l and grain boundary D_{gb} diffusion coefficients for Hf in 3Y-TZP doped with 0.5 mol% (a and b) and 1 mol% (c and d) of oxides (SIMS measurements). On (c) and (d) there are also plots for ZrO_2–10 mol% HfO_2. For comparison data from Sakka et al.[11] and Swaroop et al.[12] of Hf diffusivities in tetragonal zirconia are shown.

and samples mentioned in Table 1. The experimental results are displayed in Fig. 3 as Arrhenius plot ($D = D_0 \exp(-Q/RT)$ where D_0—pre-exponential factor, Q—activation energy, R—gas constant, T—temperature in Kelvin) of the diffusivities as a function of inverse temperature, using $\delta = 1$ nm and $s = 1$ and compared with data from Refs. 11,12. Calculated values of D_0 and Q (by the least square method (LSM)) are presented in Table 2.

There is no significant grain size growth observed in samples annealed for SIMS measurements.

Almost ideal symmetric Zr and Hf concentration distribution shown in Fig. 4 for diffusion couple of undoped 3Y-TZP and ZrO_2–10 mol% HfO_2 confirms that diffusion coefficients of these elements in zirconia are equivalent, as noticed in Ref. 26. The concentration distribution indicates preferential diffusion of the analyzed cations along grain boundaries (see Fig. 4). Such concentration distribution is described by Oishi and Ichimura's equations[27]:

$$\frac{2(c - c')}{c'' - c'} = A \ \exp(-Bx) \tag{3}$$

where

$$A = 1 - \frac{6}{\pi^2} \sum_{m=1}^{m=\infty} \left(\frac{1}{m^2}\right) \exp\left(-\frac{D_l m^2 \pi^2 t}{r^2}\right) \tag{4}$$

Table 2
Parameters of lattice and grain boundary diffusion coefficients for 0.5 and 1 mol% oxide doped 3Y-TZP, undoped 3Y-TZP and ZrO_2–10 mol% HfO_2 (SIMS).

Dopant oxide	0.5 mol%				1 mol%			
	$\log(D_{0l})$	$\log(D_{0gb})$	Q_l	Q_{gb}	$\log(D_{0l})$	$\log(D_{0gb})$	Q_l	Q_{gb}
–	−0.30 ± 2.98	−0.90 ± 3.26	591 ± 95	442 ± 104				
Al_2O_3	−13.55 ± 3.13	−8.88 ± 5.77	210 ± 100	201 ± 184	−5.08 ± 1.64	−5.67 ± 2.87	436 ± 52	275 ± 92
SiO_2	−9.69 ± 1.70	−7.21 ± 5.06	333 ± 54	257 ± 162	0.95 ± 5.51	2.38 ± 10.87	635 ± 173	536 ± 341
MgO	−11.40 ± 2.85	2.76 ± 4.73	278 ± 91	573 ± 152	−4.02 ± 2.93	0.02 ± 2.95	470 ± 94	460 ± 95
$MgAl_2O_4$	−10.09 ± 1.89	−6.16 ± 7.11	319 ± 60	282 ± 227	-3.98 ± 2.18	−4.16 ± 7.68	471 ± 68	332 ± 241
GeO_2	−9.00 ± 1.72	1.69 ± 1.82	353 ± 55	538 ± 58	−3.83 ± 1.99	1.30 ± 0.83	477 ± 63	500 ± 26
TiO_2	−12.88 ± 1.57	−9.19 ± 4.00	227 ± 50	198 ± 127	−3.26 ± 3.33	−3.17 ± 3.59	494 ± 105	365 ± 113
HfO_2					−1.43 ± 4.09	−4.59 ± 4.77	554 ± 131	310 ± 152

Where D_{0l} and D_{0gb} are pre-exponential factors respectively for lattice and grain boundary diffusion (in m^2/s) and Q_l and Q_{gb} are activation energies (in kJ/mol) respectively for lattice and grain boundary diffusion.

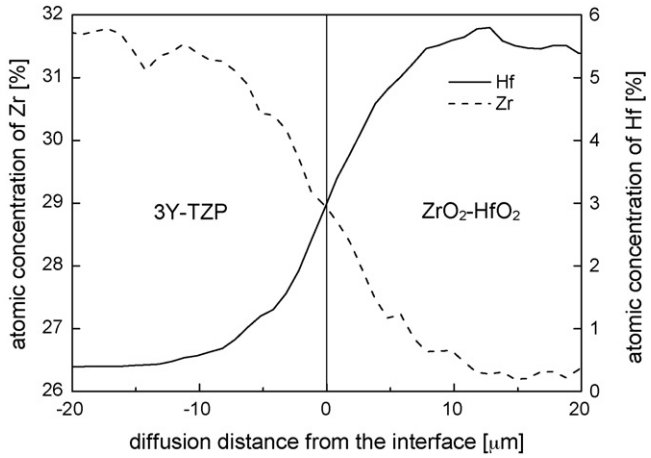

Fig. 4. Concentration distributions of Zr and Hf after interdiffusion at 1458 °C for 120 h for diffusion couple of undoped 3Y-TZP and ZrO_2–10 mol% HfO_2 (zirconia–hafnia).

$$B = \left[\frac{4D_l}{r\delta D_{gb}} \sum_{m=1}^{m=\infty} \exp\left(-\frac{D_l m^2 \pi^2 t}{r^2}\right)\right]^{1/2} \quad (5)$$

and x is the diffusion distance from the interface, c is the concentration at x, c' and c'' are the initial concentrations in both sides of diffusion couple, r is the grain radius, the rest of symbols was defined earlier.

Eq. (3) can be written in a logarithmic form as:

$$\ln\left[2\frac{c-c'}{c''-c'}\right] = \ln A - Bx \quad (6)$$

From Eq. (6) A and B were calculated with the least square method and hence values of D_l were determined by solving Eq. (4) and next D_{gb} from Eq. (5). Because of long time of diffusion annealing for EMA measurements significant grain size growth was observed in studied materials (Fig. 5). The influence of the grain size on calculated values of diffusion coefficients for pure 3Y-TZP at 1510 °C is presented in Fig. 6. One can see rather significant dependence of the diffusion coefficients in the range of considered grain sizes.

Due to grain growth the choice of value of r used in Eqs. (4) and (5) poses a problem. The grain growth during annealing can

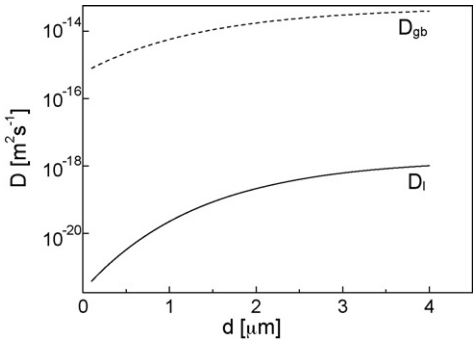

Fig. 6. The influence of grain sizes on values of diffusion coefficients calculated from Eqs. (4) and (5) for 3Y-TZP at 1510 °C.

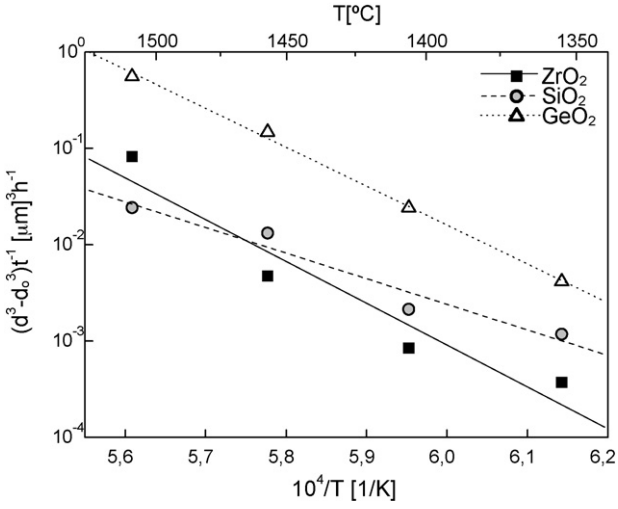

Fig. 7. The variation of kinetic constant with inverse temperature for annealed 3Y-TZP samples: pure (signed as ZrO_2) and doped by SiO_2 and GeO_2.

be described by Eq. (7)[28]:

$$d^N - d_0^N = K_{0g} t \exp\left(-\frac{Q_g}{RT}\right) \quad (7)$$

where d is the grain size after annealing time t, d_0—initial grain size, N and K_{0g}—constants and Q_g—activation energy for the grain growth.

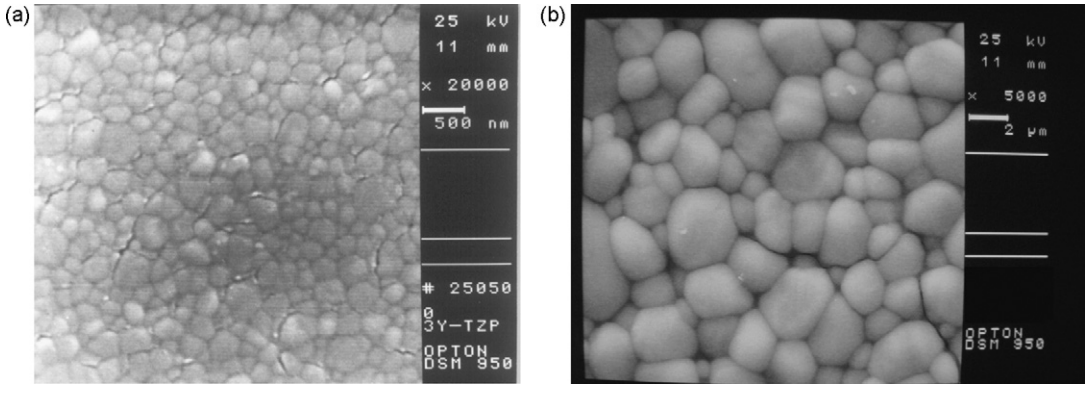

Fig. 5. SEM micrograph of microstructure of undoped 3Y-TZP before (a) and after annealing at 1510 °C for 72 h (b).

Table 3
Grain radius r in μm for undoped and 1 mol% doped 3Y-TZP and ZrO_2–10 mol% HfO_2 used in Eqs. (4) and (5).

Dopant oxide	3Y-TZP				ZrO_2–10 mol% HfO_2			
	1350 °C/312 h	1407 °C/240 h	1458 °C/120 h	1510 °C/72 h	1350 °C/312 h	1407 °C/240 h	1458 °C/120 h	1510 °C/72 h
–	0.19	0.29	0.40	0.59	0.21	0.29	0.33	0.41
Al_2O_3	0.20	0.29	0.46	0.77	0.26	0.40	0.52	0.70
SiO_2	0.28	0.37	0.42	0.49	0.28	0.35	0.38	0.42
MgO	0.35	0.46	0.51	0.59	0.48	0.48	0.49	0.49
$MgAl_2O_4$	0.43	0.56	0.63	0.73	0.39	0.44	0.47	0.52
GeO_2	0.44	0.72	0.99	1.40	0.25	0.32	0.36	0.43
TiO_2	0.48	0.60	0.64	0.72	0.22	0.27	0.30	0.35

Values of $r = d_{0.5}$ were calculated from Eq. (7) for following times: 156 h for 1350 °C, 120 h for 1407 °C, 60 h for 1458 °C and 36 h for 1510 °C.

Fig. 7 shows the variation of kinetic constant $K_g = (d^N - d_0^N)/t$ with respect to the inverse temperature for undoped and selected doped samples for $N = 3$.[28] The values of initial grain size d_0 were taken for undoped and 1 mol% doped samples from Table 1 and the values of grain size d after annealing were measured in the same way as d_0. Hence the values of K_{0g} and Q_g were obtained by LSM. The procedure described above was applied to the rest of the samples. It was decided that the value of $d = d_{0.5}$ after half of annealing time would be used for calculating the diffusion coefficients from Eqs. (4) and (5).

Obtained from Eq. (7) values of grain radius $r = d_{0.5}/2$ were collected in Table 3.

The diffusion coefficients calculated from Eqs. (4) and (5) are shown in Fig. 8 using $\delta = 1$ nm and compared with data from Refs. 11,12.

Calculated values of D_0 and Q are presented in Table 4.

Table 4
Parameters of the lattice and grain boundary diffusion coefficients for 1 mol% cation-doped 3Y-TZP and ZrO_2–HfO_2 (EMA).

Dopant oxide	$\log(D_{0l})$	$\log(D_{0gb})$	Q_l	Q_{gb}
–	−8.04 ± 2.03	−1.14 ± 2.23	389 ± 66	451 ± 73
Al_2O_3	−0.73 ± 3.01	4.28 ± 1.45	619 ± 98	608 ± 47
SiO_2	−8.12 ± 2.77	−4.75 ± 5.53	383 ± 90	322 ± 180
MgO	1.38 ± 0.32	−11.69 ± 1.42	686 ± 10	89 ± 46[a]
$MgAl_2O_4$	−12.19 ± 4.08	−1.59 ± 0.56	238 ± 132	407 ± 18
GeO_2	−0.88 ± 6.52	−2.26 ± 4.28	602 ± 212	379 ± 139
TiO_2	−8.31 ± 1.02	−7.76 ± 2.54	370 ± 33	209 ± 83

[a] This value seems to be too small.

4.2. Superplastic strain rate measurements

The variation of the strain rate $d\varepsilon/dt$ as a function of the stress σ and inverse temperature $1/T$ respectively for 3Y-TZP 1 mol% doped and undoped samples are depicted in Figs. 9 and 10. The strong influence of cation doping on superplastic strain rate can be seen. The strain rate $d\varepsilon/dt$ could be expressed as[3–5]:

$$\frac{d\varepsilon}{dt} = \frac{A_0 DGb}{kT}\left(\frac{b}{d}\right)^p\left(\frac{\sigma}{G}\right)^n \quad (8)$$

where A_0 is a dimensionless constant, D is the diffusion coefficient, G is the shear modulus, b is the Burgers vector, k is Boltzmann's constant, p is the exponent of the inverse grain size and n is the stress exponent.

The stress exponent n values (calculated for all temperatures and dopants) are in the range 1.1–3.3.

4.3. First principle calculations of the electronic states and elastic properties

The results of the first principles calculations of the C_{66} elastic constant, the net ionic charges of metal cations Q_c, oxygen anions Q_o and the average value of products of net charges Θ

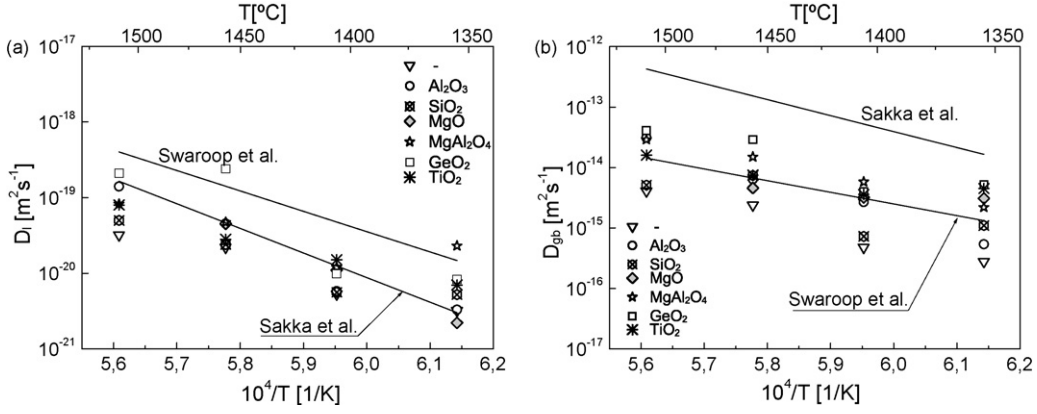

Fig. 8. Arrhenius plots of lattice D_l (a) and grain boundary D_{gb} (b) diffusion coefficients for Hf in 3Y-TZP doped with 1 mol% of cations (EMA measurements). For comparison data from Sakka et al.[11] and Swaroop et al.[12] of Hf diffusivities in tetragonal zirconia are shown.

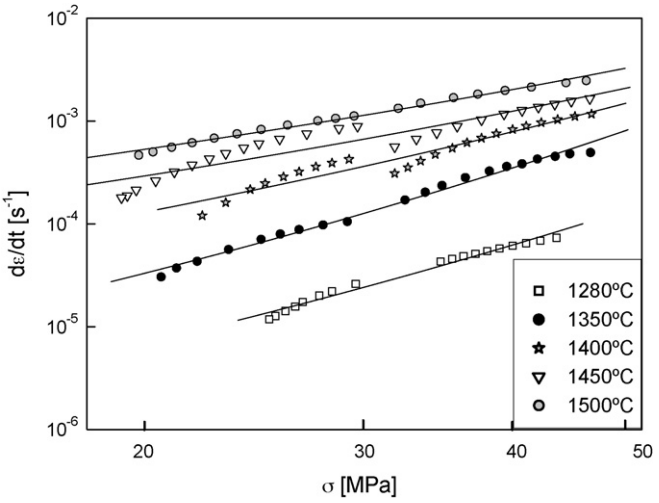

Fig. 9. Strain rate $d\varepsilon/dt$ in function of stress σ for undoped 3Y-TZP for various temperatures.

are presented in Table 5. Θ is defined according to Ref. 13 as:

$$\Theta = \frac{1}{N_b}\sum_{N_b} Q_c Q_O \tag{9}$$

where N_b is the number of cation-oxygen bonds in the first coordination sphere of the dopant atom; Q_c and Q_o are the absolute values of the net charges of cations and oxygen ions, respectively. The value of N_b is 17 for Mg (9 cations are bonded to 17 oxygens) and the number of neighbours is 18 for other cases (9 cations bonded to 18 oxygens). The parameter Θ corresponds to Coulomb's attractive force in the region where the dopant atom is located.

One has to remember that the strong dopant segregation along grain boundary in thin layer (of width about 5 nm) takes place in 3Y-TZP.[29,30] In this surface layer a dopant concentration is several times higher than in a grain interior. It is known that the grain

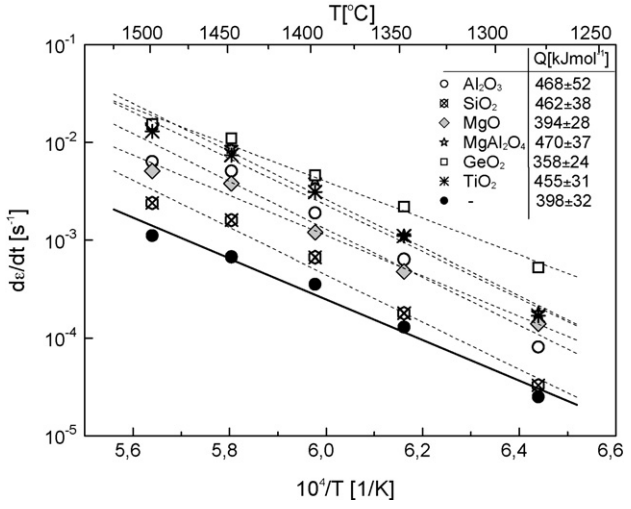

Fig. 10. Strain rate $d\varepsilon/dt$ in function of inverse temperature for undoped and 1 mol% doped 3Y-TZP for $\sigma = 30$ MPa and calculated activation energy Q for superplastic deformation. The thick solid line represents the relationship for undoped 3Y-TZP.

Table 5
Calculated values of net charges for cations Q_c, an anion (oxygen) Q_o, the average value of products of net charges Θ and C_{66} elastic constant for doped and undoped 3Y-TZP. Q_c and Q_o are in electron charge units.

Dopant	Q_c	Q_o	Θ	C_{66} (GPa)
Zr^{4+} in undoped 3Y-TZP	2.74	−1.27	2.80	177.2
Ti^{4+}	2.55	−1.23	2.76	173.1
Si^{4+}	2.49	−1.22	2.73	169.3
Ge^{4+}	2.39	−1.17	2.72	167.8
Mg^{2+}	1.70	−1.12	2.76	176.9
Mg^{2+} in $MgAl_2O_4$	1.70			
Al^{3+}	2.12	−1.16	2.69	163.7
Al^{3+} In $MgAl_2O_4$	2.13			
$Mg^{2+} + Al^{3+}$		−1.22	2.52	157.6

boundary diffusion of Zr^{4+} plays the main role in superplastic flow in 3Y-TZP.[5] Therefore the calculations for higher dopant concentration than 0.5 or 1 mol% were done. The net charges for Mg and Al were calculated for 2.8 mol% dopant concentration and the others for 6.7 mol% as explained in Section 3.

It was shown (Table 5) that the decrease of C_{66} elastic constant is accompanied by the decrease of cation and oxygen ionicity (by absolute value) and the corresponding decrease of Θ.

5. Discussion

The diffusion coefficients for 3Y-TZP samples pure and doped with 0.5 and 1 mol% of various oxide are shown in Figs. 3 and 8. Doping of 0.5 mol% causes significant decrease of the lattice diffusion coefficient D_l (above one order of magnitude in comparison with the undoped 3Y-TZP for the highest temperature) and decrease of grain boundary diffusion coefficient D_{gb} (although less significant). This effect is ambiguous because at the same time some increase of superplastic strain rate was observed.[31] In order to explain this effect two hypotheses were proposed: in the first it was assumed that strain rate was proportional to grain boundary diffusion of Zr^{4+} and dopant cation, in the second it was assumed that the strain rate is also proportional to the cavity growth. Details one can find in Ref. 31. It is not now clear why the lattice diffusion coefficients decrease for 0.5 mol% doped samples. Cations added to ZrO_2 draw neighbouring O^{2-} toward the dopant cations itself and the atomic distortion probably causes a decrease in lattice diffusion. In turn for 1 mol% doping 3Y-TZP D_l is similar to this in pure sample but D_{gb} is several times higher than in pure zirconia. Here probably the change in chemical bonding state countervails the distortion effect and no change in lattice diffusion is observed but due to dopant cation segregation (near grain boundary) grain boundary diffusion increases. There is the curvature in the Arrhenius plots in Figs. 3 and 8. This is the strongest in Fig. 3a (for lattice diffusion for 0.5 mol% doped samples) but it is also visible in the other plots. At first the experimental procedure was checked and the possibility of making of rough errors in the measurements was excluded (for instance in setting of temperature in the furnace or in collecting data by SIMS and EMA). Another possibility—it is non-Arrhenius behaviour of

the diffusivity. It appears when more than one diffusion mechanism operates simultaneously or when the change of free energy of vacancy migration and/or vacancy formation with temperature occurs due to some physical reasons (for instance for phase transformation). In the case of yttria stabilized cubic zirconia Zr self-diffusion occurs via a single vacancy mechanism, i.e. via point defect $V_{Zr}^{4'}$ (Kröger–Vink notation) as it was shown by Kilo et al.[32] and Kilo.[33] One can assume that in the case of our tetragonal zirconia the same diffusion mechanism is and Hf tracer migrates via zirconium vacancies. For calcia stabilized cubic zirconia it was assumed[33] that cation vacancies are associated with oxygen vacancies and association energies in the order of 1 eV per oxygen vacancies were estimated. It causes that the activation energy decreases in function of temperature. Maybe the similar phenomenon occurs in the case of our yttria stabilized tetragonal zirconia.

The comparison of obtained results of diffusivity for pure zirconia with literature data[11,12] shows excellent agreement, especially with data of Swaroop et al.[12] for D_{gb}. Differences between data of Sakka et al.[11] and the present ones or data by Swaroop et al.[12] result from different chemical composition of ceramics used by authors of Refs. 11,12 or by us (Sakka et al. used 14 mol% CeO_2 stabilized tetragonal zirconia). Consistence of SIMS and EMA data (Fig. 11) especially for D_{gb} confirms reliability of the present results. It should be underlined that simultaneous measurements of diffusion coefficients in one batch of tetragonal zirconia by two methods are reported for the first time.

Values of D_{gb} are greater by 4–5 orders of magnitude than for D_l and Q_l are usually larger than Q_{gb}. Diffusion coefficients for ZrO_2–10 mol% HfO_2 composite are very similar to those for pure 3Y-TZP.

As the surface diffusion can potentially contribute to the mass transport in porous materials, it is usually preferable to use samples with relative densities >99%. The samples prepared from 3Y-TZP have relative densities from 97 to 99% unlike those from ZrO_2–10 mol% HfO_2 composite which are less dense (94–98%). Very good agreement between our results and data reported by Swaroop et al.[12] (for specimens with relative densities > 99%) for pure 3Y-TZP can be seen in Fig. 11a. It should be noticed that Swaroop et al.[12] reports the value of theoretical density of 3Y-TZP equal to 6.03 g/cm^3, but we used 6.1 g/cm^3. For choice of Ref. 12 the relative density of our pure 3Y-TZP equals 99% and it suggests that the initial densities of samples used by Swaroop et al.[12] and by us are almost the same. During long annealing time the samples for EMA measurements should attain the theoretical density.[28,34] As it was noticed previously EMA and SIMS results (of D_{gb}) are similar thus the influence of small porosity of samples used in the present studies is insignificant for the diffusion coefficients.

Another problem which requires attention is the solubility limit of the added oxides in ZrO_2 and the influence of the second phase on diffusion coefficients. From Refs. 35–37 it is known that GeO_2, TiO_2 and MgO have the solubility limit in $ZrO_2 > 1$ mol%. But SiO_2 and Al_2O_3[38,39] have solubility limit about 0.6 mol%. We are not aware of any strict information about solubility of $MgAl_2O_4$ in ZrO_2 however based on some reports, for instance,[40] one can conclude that it is close to Al_2O_3. The second phase locates at multiple grain junction as glass pockets[38] for SiO_2 or alumina grains[39] and there is no amorphous phases along grain boundaries. Then the grain boundary diffusion of Hf ions in doped by SiO_2, Al_2O_3 or $MgAl_2O_4$ 3Y-TZP should not depend on the second phase precipitation. Only the dopant cations which segregates in grain boundaries could influence the diffusion.

The dependence of grain boundary diffusion coefficient D_{gb} on the net charges of cations and oxygen is presented in Fig. 12. The plots in Fig. 12 show that grain boundary diffusivity increases when ionic bond strength Θ and the ionicities of cations and anions decrease by absolute values. The plots in Fig. 12 are analogous to the results presented for doped alumina ceramics in Ref. 41. For zirconia one can find first-principles molecular orbital calculations only for GeO_2 and TiO_2 doped samples.[13,42] Results of net charge calculations for Ge^{4+}, Ti^{4+} and O^{2-} (Table 5) are similar to those obtained in Refs. 13,42. The change of C_{66} elastic values in function of dopant cation are not significant (Table 5). It means that changes in shear modulus G (which is proportional to C_{66}) do not influence the superplastic strain rate (Eq. (8)) and mainly the changes of D_{gb} are important.

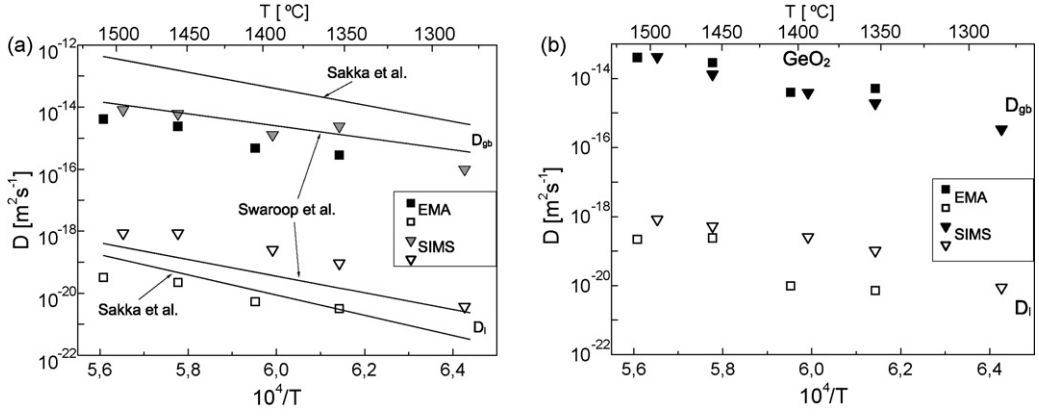

Fig. 11. Comparison of the lattice (empty symbols) and grain boundary (full symbols) diffusion coefficients obtained with two methods in pure 3Y-TZP (the literature data are added for comparison) (a) and in GeO_2 doped 3Y-TZP (b). For other dopants both results are very similar.

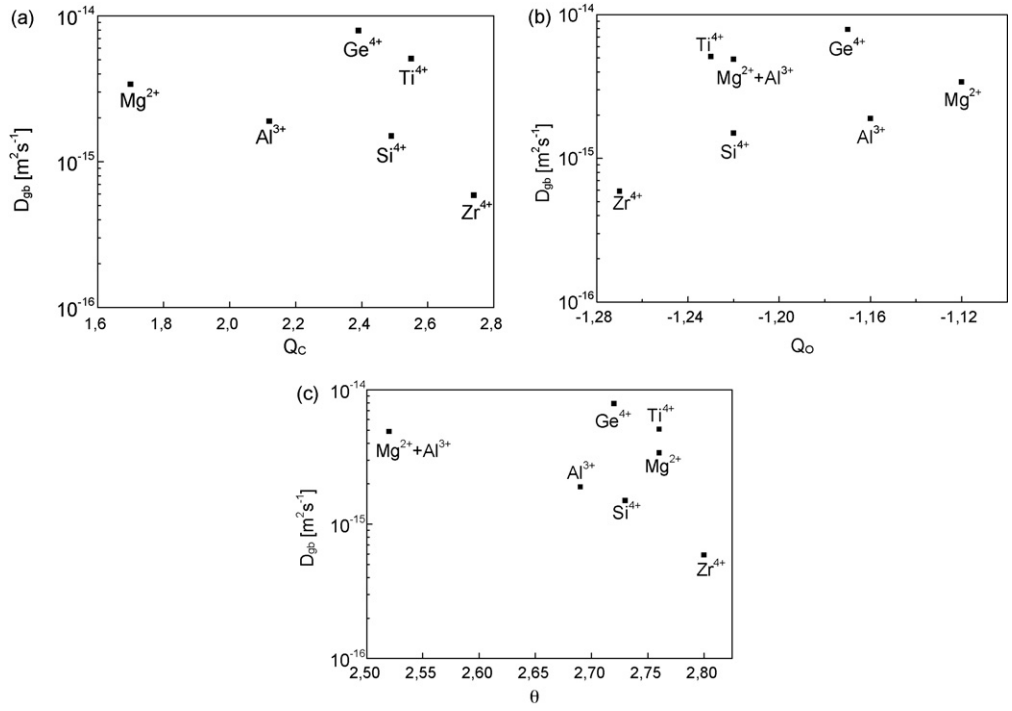

Fig. 12. The grain boundary diffusion coefficient D_{gb} (EMA measurements) for undoped and 1 mol% doped 3Y-TZP at 1400 °C against a value of Q_c (a), Q_o (b) and θ (c). Zr^{4+} means undoped 3Y-TZP. Q_c and Q_o are in electron charge units.

According to Ref. 5 the superplastic flow in 3Y-TZP is attributed to the grain boundary sliding controlled by grain boundary diffusion of Zr^{4+} ions. The relationship between grain boundary diffusion coefficient and superplastic strain rate at various temperatures for 30 MPa for doped 3Y-TZP is shown in Fig. 13. The linear relationship in Fig. 13 is consistent with earlier assumptions[5] and Eq. (8). Using the slope S obtained from Fig. 13 the unknown parameter A_0 in Eq. (8) was calculated from Eq. (10) (obtained after Eq. (8) transformation) for $n=2$ and $p=2$ for various temperatures ($n=2$ is the average value of 35 obtained results, but $p=2$ was taken from[43]):

$$A_0 = \frac{SkTd^2G}{b^3\sigma^2} \tag{10}$$

The following values of parameters in Eq. (10) were used.

$k = 1.38 \times 10^{-23}$ J/K, $d = 0.3$ μm (Table 1), $G = 1.54 \times 10^5 - 35.2 \times T$ (MPa),[44] $b = 0.36$ nm[5], $\sigma = 30$ MPa ($d = 0.3$ μm was taken because, for example a standard deviation of grain size for undoped 3Y-TZP equals 0.06 (Table 1); all grain size values for 1 mol% doped samples are in the range of 0.24–0.36 μm).

The value of the slope S (from Fig. 13) equals about 5.7×10^{11} m^{-2} and hence the value of $A_0 \approx 2.7 \times 10^3$ was calculated from Eq. (10). The Eq. (8) can be written as:

$$\frac{d\varepsilon}{dt} = 2.7 \times 10^3 \frac{Db^3\sigma^2}{kTd^2G} \tag{11}$$

where $D = D_{gb(Zr)}$ in m^2/s, G and σ should be given in Pa, d and b in m, T in K.

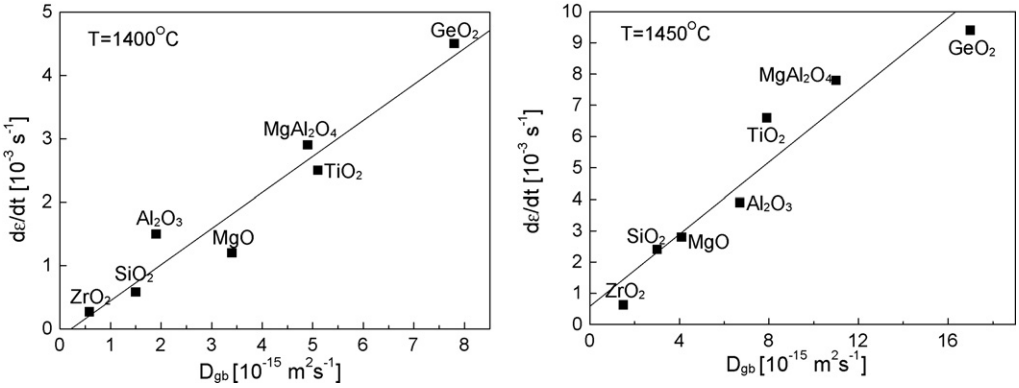

Fig. 13. The strain rate $d\varepsilon/dt$ versus grain boundary diffusion coefficient D_{gb} (EMA measurements) for undoped and 1 mol% doped 3Y-TZP at two temperatures for 30 MPa. The values of D_{gb} were calculated from the Arrhenius plots using parameters from Table 4.

For pure 3Y-TZP $D_{gb(Zr)} = 7.2 \times 10^{-2} \exp(-451{,}000/RT)$ (m^2/s) (Table 4) and Eq. (11) can be written as:

$$\frac{d\varepsilon}{dt} = B_0 \frac{\sigma^2}{Td^2G} \exp\left(-\frac{451,000}{RT}\right) \quad (12)$$

where $B_0 = 6.6 \times 10^{-4}\ m^2\ K\ Pa^{-1}\ s^{-1}$.

If we plotted Fig. 13 using the individual points of D_{gb} from Fig. 8b we would obtain the values of slopes S which equalled 6.2×10^{11} and $3.0 \times 10^{11}\ m^{-2}$ accordingly at 1400 and 1450 °C. The value of $S = 5.7 \times 10^{11}\ m^{-2}$ taken here was obtained using values of D_{gb} calculated from Arrhenius relationship using parameters from Table 4. As it is shown there are not significant differences among these values of S. In Ref. 43 the constitutive Eq. (13) was derived for pure Y_2O_3-stabilized zirconia:

$$\frac{d\varepsilon}{dt} = B_M \frac{(\sigma - \sigma_0)^2}{Td^2} \exp\left(-\frac{460,000}{RT}\right) \quad (13)$$

where $B_M = 3 \times 10^{10}\ \mu m^2\ K\ MPa^{-2}\ s^{-1}$ and threshold stress $\sigma_0 = 5 \times 10^{-4}(\exp(120{,}000/RT))/d$ in MPa.[43]

The curves calculated from Eqs. (12) and (13) for $d = 0.3\ \mu m$ are compared between each other and with experimental data in Fig. 14. Our relationship (Eq. (12)) predicts well the superplastic strain rate in function of stress in the whole range of applied temperature, but the Eq. (13) proposed by Jimenez-Melendo et al.[43] seems to be not good at the lowest temperature because of the high value of threshold stress σ_0 at 1280 °C (about 18 MPa).

Authors tried to determine the threshold stress σ_0 for superplasticity results (Fig. 9) by plotting the experimental data in the form $(d\varepsilon/dt)^{1/n}$ versus σ on a linear scale. The extrapolations of the linear least squares fit of the data (for all temperatures) to zero strain rate gave the negatives values of σ_0 and these results are not physically realistic. We obtained the similar results for other doped 3Y-TZP. In our case the longest time of heating samples during superplastic tests was about 3 h (for 1280 °C) then the grain growth was insignificant and it could not influence our

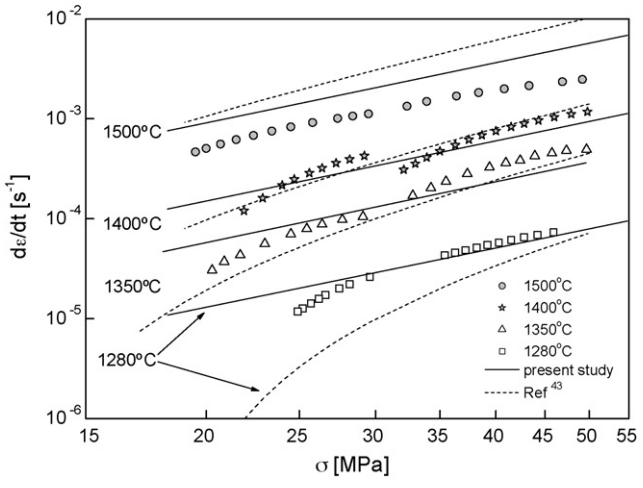

Fig. 14. The comparison of the strain rate Eq. (12) for pure 3Y-YZP obtained here with Eq. (13) proposed by Jimenez-Molendo et al.[43] for $d = 0.3\ \mu m$ for various temperatures (experimental data were taken from Fig. 9).

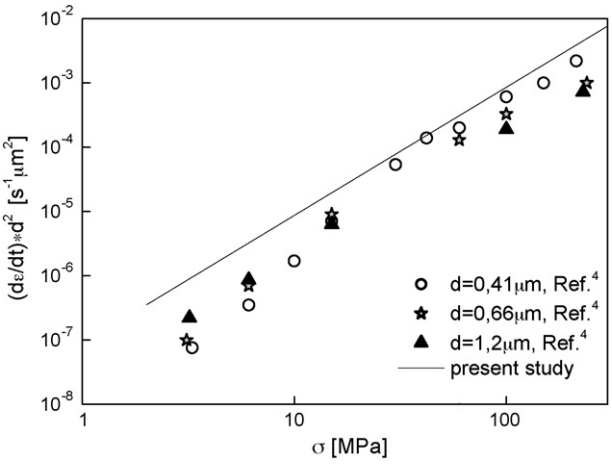

Fig. 15. Grain-size-compensated strain rate versus stress at 1450 °C for 3Y-TZP from Ref. 4. Data were obtained in compression test for samples with various initial grain sizes (shown in the legend). Solid line was calculated from multiplied by d^2 Eq. (12).

data. It seems to us that because values of σ_0 are rather small in comparison with applied in tests stresses it is difficult to obtain them precisely from the experimental data.

In Fig. 15 strain rate data for 3Y-TZP at $T = 1450$ °C taken from Ref. 4 were presented in comparison with the line calculated from multiplied by d^2 Eq. (12). Our relationship (Eq. (12)) described well Owen and Chokshi[4] data for stresses above 30 MPa, but below $\sigma = 30$ MPa stress exponent n seems to be bigger than 2 (accordingly to Ref.4 for low stresses $n \approx 3$). Another reason of no compatibility between our relationship and the cited data at low stresses is a significant grain growth in long-time tests in Ref. 4. For instance: the final grain size of a sample with initial grain size $d = 0.41\ \mu m$ tested at $\sigma = 3.3$ MPa for about 156 h equalled 0.95 μm,[4] but in Fig. 15 the initial grain sizes were used for calculations of $(d\varepsilon/dt)d^2$.

6. Summary and conclusions

In the present paper we report on diffusion measurements of Hf^{4+} ions in 3 mol% Y_2O_3 stabilized tetragonal zirconia (3Y-TZP) doped with 0.5 and 1 mol% of various oxides as: Al_2O_3, SiO_2, MgO, $MgAl_2O_4$, GeO_2 and TiO_2. The measurements were done by two methods: (1) by SIMS for establishing tracer (Hf) diffusion profiles from thin layers of HfO_2 and (2) by electron microprobe analyser (EMA) for evaluating diffusion profiles in the cross-section of 3Y-TZP and ZrO_2–10 mol% HfO_2 joints (Zr–Hf interdiffusion) for 1 mol% doped samples. For samples doped 0.5 mol% measurements were done only by SIMS. For both cases Hf was used as a tracer, which enabled to evaluate the matrix cation diffusivity. We have shown that the diffusivity of Hf ions in 3Y-TZP is the same as for Zr ions. The superplastic strain rate versus stress and the inverse temperature were also measured. First principle calculations of the electronic states of Zr^{4+}, dopant cations and O^{2-} and elastic properties in 3Y-TZP are reported to interpret experimental results. The general conclusions of the present studies are:

- For addition of 0.5 mol% of dopants the lattice diffusion coefficient D_l and the grain boundary diffusion coefficient D_{gb} decreased in comparison with pure 3Y-TZP. For 1 mol% doped samples D_l remains unchanged, however D_{gb} increased several times. Superplastic strain rate of 3Y-TZP is significantly enhanced by cation doping.
- For undoped and 1 mol% doped samples both measurement methods gave similar results. Additionally the results for pure 3Y-TZP are close to data given by Swaroop et al.[12] for the same ceramics.
- The net charge of Zr^{4+}, dopant cations, and O^{2-} and average value of products of net charges (corresponding to a Coulomb's attractive force) calculated by the first principle method are correlated with the values of the grain boundary diffusion coefficient. These relationships show that enhancement of the grain boundary diffusion coefficient D_{gb} results from the reduction of ionic bonding strength between cation and oxygen ion in doped 3Y-TZP.
- The new constitutive equation for superplastic flow of yttria-stabilized tetragonal zirconia ceramics was proposed.

Acknowledgements

This work was supported by the Polish Ministry of Science and Higher Education under Grant No. 3T08D 013 29 during the years 2005–2008. The authors thank Mgr Władysław Wesołowski for preparing samples for diffusion measurements and making graphs for this publication, Dr Rafał Jakieła for making diffusion measurements, Dr Marek Rećko for preparing computer programs for diffusion coefficient calculations, and Mgr Andrzej Gładki for grain size measurements. The authors acknowledge CPU time allocation at Interdisciplinary Center for Mathematical and Computer Modelling, Warsaw University (Grant No. G28-22).

References

1. Pampuch, R., *Ceramic Materials, Outline of Science of Inorganic and Non-metallic Materials*. PWN, Warsaw, 1988, p. 434.
2. Wakai, F., Sakaguchi, S. and Matsuno, Y., Superplasticity of yttria-stabilized tetragonal ZrO_2 polycrystals. *Adv. Ceram. Mater.*, 1986, **1**, 259–263.
3. Chokshi, A. H., Superplasticity in fine grained ceramics composites: current understanding and future prospects. *Mater. Sci. Eng.*, 1993, **A166**, 119–133.
4. Owen, D. M. and Chokshi, A. H., The high temperature mechanical characteristics of superplastic 3 mol% yttria stabilized zirconia. *Acta Mater.*, 1998, **46**, 667–679.
5. Berbon, M. Z. and Langdon, T. G., An examination of the flow process in superplastic yttria-stabilized tetragonal zirconia. *Acta Mater.*, 1999, **47**, 2485–2495.
6. Charit, I. and Chokshi, A. H., Experimental evidence for diffusion creep in the superplastic 3 mol% yttria-stabilized tetragonal zirconia. *Acta Mater.*, 2001, **49**, 2239–2249.
7. Boniecki, M., Librant, Z., Gładki, A., Węglarz, H. and Wesołowski, W., Superplastic flow in 3 mol% yttria-stabilized zirconia at high temperatures. *Key Eng. Mater.*, 2002, **206–213**, 1013–1016.
8. Kim, B. N., Hiraga, K., Morita, K. and Sakka, Y., A high-strain-rate superplastic ceramics. *Nature*, 2001, **413**, 288–291.
9. Miramuda, J., Nakano, M., Sasaki, K., Ikuhara, Y. and Sakuma, T., Effect of cation doping on the superplastic flow in yttria-stabilized tetragonal zirconia polycrystals. *J. Am. Ceram. Soc.*, 2001, **84**(8), 1817–1821.
10. Nakatani, K., Nagayama, H., Yoshida, H., Yamamoto, T. and Sakuma, T., The effect of grain boundary segregation on superplastic behavior in cation-doped 3Y-TZP. *Scripta Mater.*, 2003, **49**, 791–795.
11. Sakka, Y., Oishi, Y., Ando, K. and Morita, S., Cation interdiffussion and phase stability in polycrystalline tetragonal ceria–zirconia–hafnia solid solution. *J. Am. Ceram. Soc.*, 1991, **74**(10), 2610–2614.
12. Swaroop, S., Kilo, M., Argirusis, C., Borchardt, G. and Chokshi, A., Lattice and grain boundary diffusion of cations in 3YTZ analyzed using SIMS. *Acta Mater.*, 2005, **53**, 4975–4985.
13. Kuwabara, A., Nakano, M., Yoshida, H., Ikuhara, Y. and Sakuma, T., Superplastic flow stress and electronic structure in yttria-stabilized tetragonal zirconia polycrystals doped with GeO_2 and TiO_2. *Acta Mater.*, 2004, **52**, 5563–5569.
14. Venkatachari, K. R. and Raj, R., Superplastic flow in fine-grained alumina. *J. Am. Ceram. Soc.*, 1986, **69**(2), 135–138.
15. Kohn, W. and Sham, L. J., Self-consistent equations including exchange and correlation effects. *Phys. Rev.*, 1965, **140**, 1133–1138.
16. Soler, J., Artacho, E., Gale, J. D., García, A., Junquera, J., Ordejón, P. *et al.*, The SIESTA method for ab initio order –N materials simulation. *J. Phys. Condens. Matter*, 2002, **14**, 2745–2779.
17. Perdew, J. P., Chevary, J. A., Vosko, S. H., Jackson, K. A., Pederson, M. R., Singh, D. J. *et al.*, Atoms, molecules, solids, and surfaces: applications of the generalized gradient approximation for exchange and correlation. *Phys. Rev. B*, 1992, **46**, 6671–6687.
18. Troullier, N. and Martins, J. L., Efficient pseudopotentials for plane-wave calculations. *Phys. Rev. B*, 1991, **43**, 1993–2006.
19. Perdew, J. P., Burke, K. and Ernzerhof, M., Generalized gradient approximation made simple. *Phys. Rev. Lett.*, 1996, **77**, 3865–3868.
20. Natanson, Y., Boniecki, M. and Łodziana, Z., Influence of elastic properties on superplasticity in doped yttria-stabilized zirconia. *J. Phys. Chem. Sol.*, 2009, **70**, 15–19, doi:10.1016/j.jpcs.2008.08.014.
21. Nielsen, H. and Martin, R. M., First-principles calculation of stress. *Phys. Rev. Lett.*, 1983, **50**, 697–700.
22. Yao, H., Ouyang, L. and Ching, W.-Y., Ab initio calculation of elastic constants of ceramic crystals. *J. Am. Ceram. Soc.*, 2007, **90**(10), 3194–3204.
23. http://www.home.uni-osnabrueck.de/apostnik/download.html.
24. Kaur, I. and Gust, W., *Fundamentals of Grain and Interphase Boundary Diffusion*. Ziegler Press, Stuttgart, 1989, p. 422.
25. Mishin, Y., Herzig, Chr., Bernardini, J. and Gust, W., Grain boundary diffusion: fundamentals to recent developments. *Int. Mater. Rev.*, 1997, **42**, 155–177.
26. Oishi, Y., Sakka, Y. and Ando, K., Cation interdiffusion in polycrystalline fluorite-cubic solid solution. *J. Nucl. Mater.*, 1981, **96**, 23–28.
27. Oishi, Y. and Ichimura, H., Grain boundary enhanced interdiffusion in polycrystalline CaO-stabilized zirconia system. *J. Chem. Phys.*, 1979, **71**(12), 5134–5139.
28. Chokshi, A. H., Densification and high temperature deformation in oxide ceramics. *Key Eng. Mater.*, 2009, **395**, 39–54.
29. Ikuhara, Y., Thavorniti, P. and Sakuma, T., Solute segregation at grain boundaries in superplastic SiO_2-doped TZP. *Acta Mater.*, 1997, **45**, 5275–5284.
30. Nagayama, H., Kuwabara, A., Yoshida, H. and Sakuma, T., Superplastic behavior in small amount of Ge–Ti-doped TZP. *Mater Sci. Forum*, 2004, **447–448**, 365–372.
31. Boniecki, M., Jakieła, R., Librant, Z., Rećko, M. and Wesołowski, W., The influence of some oxides on the superplastic flow and diffusion in ZrO_2. In *Proc. 10th ECerS Conf.*, ed. J. G. Heinrich and C. Aneziris, 2007, pp. 1083–1088.
32. Kilo, M., Borchardt, G., Lesage, B., Kaitasov, O., Weber, S. and Scherrer, S., Cation transport in yttria stabilized cubic zirconia: ^{96}Zr tracer diffusion in $(Zr_xY_{1-x})O_{2-x/2}$ single crystals with $0.15 \leq x \leq 0.48$. *J. Eur. Ceram. Soc.*, 2000, **20**, 2069–2077.
33. Kilo, M., Cation transport in stabilised zirconias. *Defect Diffus. Forum*, 2005, **242–244**, 185–253.
34. Wang, X.-H., Chen, P.-L. and Chen, I.-W., Two-step sintering of ceramics with constant grain size. I. Y_2O_3. *J. Am. Ceram. Soc.*, 2006, **89**(2), 431–437.
35. Kim, D.-J., Jang, J.-W., Jung, H.-J., Hun, J.-W. and Yang, I.-S., Determination of solubility limit of GeO_2 in 2 mol% Y_2O_3-stabilized tetragonal ZrO_2 by Raman spectroscopy. *J. Mater. Sci. Lett.*, 1995, **14**, 1007–1009.

36. Bannister, M. and Barnes, J., Solubility of TiO_2 in ZrO_2. *J. Am. Ceram. Soc.*, 1986, **69**(11), C-269–C-271.
37. Rong, T., Huang, X. X., Wang, S. W., Zhao, S. K. and Guo, J. K., State of magnesia in magnesia (10.4 mol%)-doped zirconia powder prepared from coprecipitation. *J. Am. Ceram. Soc.*, 2002, **85**(5), 1324–1326.
38. Morita, K., Hiraga, K. and Kim, B.-N., Effect of minor SiO_2 addition on the creep behavior of superplastic tetragonal ZrO_2. *Acta Mater.*, 2004, **52**, 3355–3364.
39. Suzuki, T. S., Sakka, Y., Morita, K. and Hiraga, K., Enhanced superplasticity in an alumina containing zirconia prepared by colloidal processing. *Scripta Mater.*, 2000, **43**, 705–710.
40. Morita, K., Hiraga, K. and Kim, B.-N., High-strain superplastic flow in tetragonal ZrO_2 polycrystal enhanced by the dispersion of 30 vol.% $MgAl_2O_4$ spinel particles. *Acta Mater.*, 2007, **55**, 4517–4526.
41. Yoshida, H., Hashimoto, S. and Yamamoto, T., Dopant effect on grain boundary diffusivity in polycrystalline alumina. *Acta Mater.*, 2005, **53**, 433–440.
42. Yoshida, H., Morita, K., Kim, B.-N. and Hiraga, K., Ionic conductivity of tetragonal ZrO_2 polycrystal doped with TiO_2 and GeO_2. *J. Eur. Ceram. Soc.*, 2009, **29**, 411–418.
43. Jimenez-Melendo, M., Dominguez-Rodriguez, A. and Bravo-Leon, A., Superplastic flow of fine-grained yttria-stabilized zirconia polycrystals: constitutive equation and deformation mechanism. *J. Am. Ceram. Soc.*, 1998, **81**(11), 2761–2776.
44. Cannon, R. and Langdon, T. G., Review: creep of ceramics. Part 2. An examination of flow mechanisms. *J. Mater. Sci.*, 1988, **23**, 1–20.